ACS Catalysis

Research Article

pubs.acs.org/acscatalysis

Probing the Surface Sites of CeO_2 Nanocrystals with Well-Defined Surface Planes via Methanol Adsorption and Desorption

Zili Wu,*[,†,‡] Meijun Li,[†] David R. Mullins,[†] and Steven H. Overbury*[,†,‡]

[†]Chemical Science Division, [‡]Center for Nanophase Materials Sciences, Oak Ridge National Laboratory, Oak Ridge, Tennessee 37831, United States

ABSTRACT: Methanol has been considered as a "smart" molecule in studying the surface sites of metal oxide catalysts. In this work, methanol was utilized to probe the nature of surface sites of ceria nanocrystals with defined surface planes (nanoshapes), including rods (containing {110}), cubes ({100}), and octahedra ({111}). The adsorption and desorption of methanol were followed by in situ IR and Raman spectroscopy as well as mass spectrometry. Upon methanol adsorption at room temperature, on-top, bridging and three-coordinate methoxy species are formed on the surface of rods and cubes, whereas only on-top methoxy is present on the octahedra surface. The distribution of the methoxy species is believed to be determined not only by the coordination status of surface Ce cations but also by the number of defect sites on the three nanoshapes. During the desorption process, the methoxy species are gradually dehydrogenated into H_2 and CO via formate species as intermediates on the three ceria surfaces. A second intermediate, formyl species is also evident on the rods' surface. The methoxy species are more reactive and less stable on the rods' surface, which results in desorption of H_2 and CO at lower temperature (<583 K) than on cubes and octahedra. A higher than stoichiometric H/CO ratio is observed in the methanol-TPD products, attributed to the retention of some amount of formate and carbonate species on the ceria nanoshapes, as revealed by in situ IR. A small amount of methanol and formaldehyde desorbs at low temperature (<423 K) on the three surfaces as a result of the disproportionation reaction of the methoxy species. The UV Raman and IR results indicate that the ceria nanoshapes are slightly reduced at room temperature upon methanol adsorption and become more reduced at higher temperatures during methanol desorption. The degree of reduction is found to be dependent on the surface structure of the ceria nanoshapes.

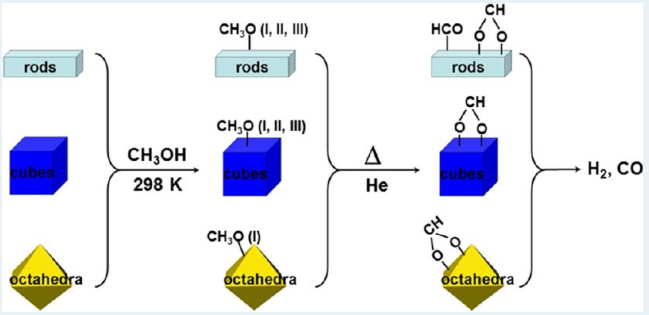

KEYWORDS: *ceria nanoshapes, rods, cubes, octahedra, surface sites, methanol adsorption and desorption, in situ spectroscopy*

1. INTRODUCTION

Thanks to its excellent redox property and high oxygen storage capacity (OSC), cerium oxide has been extensively studied as a catalyst and catalyst support for use in a variety of catalytic reactions.[1−9] To further improve the reactivity of ceria, there have been intense investigations devoted to increasing its OSC, such as doping with Zr.[1,10] With recent advances in nanomaterial synthesis, an alternative way to enhance the OSC of ceria has been made possible by manipulating the surface structure of ceria nanocrystals.[11−18] For example, ceria rods and cubes, exposing reactive crystal planes of {110} and {100}, respectively, were shown to have a much higher OSC than {111}-facet-dominated ceria polyhedra.[12,19] This was attributed to the participation of not only the surface but also the bulk in oxygen storage of both rods and cubes, whereas only the surface is involved for polyhedra. These ceria nanoshapes have also shown surface structure-dependent catalytic behavior, such as in CO oxidation and H_2 oxidation.[14,20] To understand this structure dependence, a prerequisite is the full characterization of the surface sites of these nanocrystals during the redox process. The surface defect sites of the ceria nanoshapes, including rods, cubes, and octahedra ({111}), have been characterized recently by Raman spectroscopy combined with O_2 probing.[21] UV Raman spectroscopy[21,22] was able to identify two types of defect sites on the ceria nanocrystals: Frenkel-type intrinsic defects and Ce^{3+}-related O vacancies. The nature of the reduction-induced O vacancy was revealed by Raman O_2 adsorption to be different on the three nanocrystals. For example, the rods, with the lowest surface oxygen vacancy formation energy, exhibit more clustered O vacancies than the cubes and octahedra. However, one remaining uncertainty in that study is the nature on the surface sites of these ceria nanoshapes under oxidizing conditions because no adsorbed O_2 species was observed on the oxidized surfaces. In this study, we probe the surface sites of these ceria nanoshapes using methanol.

Special Issue: Operando and In Situ Studies of Catalysis

Received: July 13, 2012
Revised: August 28, 2012
Published: September 17, 2012

Methanol has been shown to be an excellent probe molecule for the nature of the surface sites of ceria catalysts.[2,23−27] It dissociates on the surface to form methoxy species whose structure is dependent on the nature of the surface sites, that is, the coordination status of surface Ce cations and the presence of O vacancies.[2] Three types of surface methoxy species have been identified by IR spectroscopy from methanol adsorption on ceria, characterized by the different C−O stretching frequencies: around 1110 cm^{-1} for on-top methoxy (type I), around 1050 cm^{-1} for bridging methoxy (type II), and about 1020 cm^{-1} for three-coordinate methoxy (type III).[2,23] From the variation in surface structure of the three low-index CeO_2 surfaces,[28] it is expected that methanol would show different adsorption behavior and thus provide information on the nature on the real surface sites of these ceria nanocrystals.

The surface sites on ceria single crystals or thin films with {111} and {100} terminations were probed by methanol adsorption in surface science studies,[29−33] complemented by several theoretical investigations;[34−36] however, the interaction between methanol and ceria nanoparticles with well-defined surface facets is yet to be investigated under realistic conditions.[37] Furthermore, the desorption/decomposition behavior of methanol is also expected to be surface-dependent because the reaction chemistry is determined by the redox property of the ceria surface as well as the extent of the coordinative unsaturation of the Ce cations.[2,23,34,35] Therefore, the objective of this paper is 2-fold: (1) to probe the nature of surface sites on oxidized ceria nanoshapes via methanol adsorption and (2) to investigate the surface chemistry of methanol in regard to its adsorption, desorption, and oxidation pathways on the differently structured ceria nanocrystals. Our main approach is in situ vibrational spectroscopy (IR and Raman) combined with mass spectrometry. The results show that methanol interacts with the ceria surface to give three types of methoxy species, whose type and distribution are dependent on the shape of the ceria nanocrystals. Upon temperature-programmed desorption, the gas phase products (by mass spectrometer) as well as surface intermediates (by IR and Raman spectroscopy) are identified on the rods, cubes and octahedra. The adsorption and desorption behavior of methanol is determined by the surface structure and the nature of the defect sites on the ceria nanoshapes.

2. EXPERIMENTAL SECTION

2.1. Material Synthesis. The synthesis of the three ceria nanoshapes has been described in detail recently.[20,21] Briefly, CeO_2 octahedra, rods, and cubes were prepared by a hydrothermal process[12,13] in Teflon-lined stainless steel autoclaves at different hydrothermal temperatures and durations. For CeO_2 octahedra, 0.434 g of $Ce(NO_3)_3{\cdot}6H_2O$ (ARCOS, 99.50%) and 0.0038 g of $Na_3PO_4{\cdot}12H_2O$ (EM Science) precursors were used. For rods and cubes, 0.868 g of $Ce(NO_3)_3{\cdot}6H_2O$ and 9.6 g of NaOH (BDH) were used as precursors. After the hydrothermal treatment, fresh white precipitates were separated by centrifugation and washed with deionized water and ethanol several times, followed by drying at 333 K in air overnight. Nitrate species were detected on ceria rods and cubes and phosphate species were detected on octahedra by Raman spectroscopy.[21] The amount of P on the ceria octahedra surface was determined by XPS to be small (P/Ce atomic ratio around 0.16). Although P has been found to be detrimental to the redox property of ceria catalysts, a previous study indicated that the effect is relatively limited at an XPS P/Ce ratio <0.2 (corresponding to bulk P/Ce < 0.03).[38]

2.2. Material Characterizations. Measured XRD patterns and electron microscopy images of the three ceria polymorphs were similar to those reported in our previous work[20,21,39] and for brevity are not shown here. The mean particle sizes, determined from the Scherrer equation, are 11, 43, and 83 nm for rods, cubes, and octahedra, respectively. The high resolution electron micrographs of the nanoshapes[21] show the cube and octahedra shapes from which {100} and {111} terminations, respectively, are inferred, in agreement with previous studies of ceria nanomaterials.[11−13] Although previous work[11−13] has concluded that the rods consist of a mixture of {110} and {100} surfaces, the micrographs[21] showed that the rods used in our study are also characterized as having a higher concentration of defect areas than the cubes and octahedra, likely due to the presence of concentrated coordinatively unsaturated (cus) sites. Here, we consider ceria rods representative of {110} facets with the presence of cus sites. Brunauer−Emmett−Teller (BET) surface areas of the ceria nanocrystals, calcined at 673 K, were measured via nitrogen adsorption at 77 K using a Micromeritic Gemini 275 system. The BET surface areas of the rods, cubes, and octahedra are 93, 29, 12 m^2/g, respectively.

2.3. Temperature-Programmed Desorption (TPD) of Methanol. Methanol-TPD over the three ceria samples (~30 mg) was conducted on a plug−flow, temperature-controlled microreactor system (Altamira AMI 200). The ceria sample was pretreated in flowing 5% O_2/He (30 mL/min) at 673 K for 1 h, cooled to room temperature under the same atmosphere, and then switched to He purging for 30 min. The pretreated sample was exposed to methanol/He (30 mL/min He flowing through a methanol saturator kept at room temperature) for 5 min and then purged with He at room temperature for 1 h. The sample was then heated (10 K/min) up to 700 K in flowing He (30 mL/min) and held for another 30 min. The gas stream was analyzed by an online quadrupole mass spectrometer (QMS) (OmniStar GSD-301 O2, Pfeiffer Vacuum). The m/e values used to detect the different desorption products were 31 (CH_3OH), 30 (H_2CO), 45 (CH_3OCH_3), 44 (CO_2), 28 (CO), 18 (H_2O), and 2 (H_2).

2.4. In Situ IR and Raman Spectroscopy. IR spectra were collected using a Thermo Nicolet Nexus 670 spectrometer in diffuse reflectance mode (DRIFTS).[40−42] A Pike Technologies HC-900 DRIFTS cell with nominal cell volume of 6 cm^3 was used. The ceria sample (~40 mg) was pretreated in the DRIFTS cell in flowing 2% O_2/He (25 mL/min) at 673 K for 1 h and then cooled to room temperature before switching to He. A methanol (Sigma-Aldrich, >99.9%) saturator was used to deliver pulses of methanol to the sample and was kept at room temperature with 25 mL/min He bubbling through it. One pulse of methanol/He was brought to the sample by He (25 mL/min) via a 6-way valve (loop volume ~ 0.5 mL), and a series of IR spectra were collected after the pulse at room temperature. A single pulse contains ~1.7 mmol of methanol, more than sufficient to saturate the surface of the sample. About 15 min after initiating a pulse, when the IR spectra showed no further changes, the sample was heated in He (25 mL/min) to 673 K (10 K/min) and held for 30 min to complete the desorption of adsorbed methanol species. IR spectra were recorded continuously during the desorption process. All reported IR spectra are difference spectra referenced to a background spectrum collected at room

temperature after pretreatment but prior to methanol adsorption.

Methanol adsorption was also monitored by in situ Raman spectroscopy. The ceria sample was pretreated in a Raman catalytic reactor (Linkam CCR1000) in flowing 2% O_2/He (30 mL/min) at 673 K for 1 h and cooled to room temperature by purging with He (30 mL/min). The sample was then exposed to a methanol/He flow (30 mL/min of He flowing through methanol saturator at room temperature) for 5 min at room temperature and followed by purging with He. The sample was then ramped (10 K/min) up to 673 K in a He flow. Raman spectra were collected during the methanol adsorption and desorption processes. Raman scattering was collected via a customized ellipsoidal mirror and directed by a fiber optic bundle (Princeton Instruments) to the spectrograph stage of a triple Raman spectrometer (Princeton Instruments Acton Trivista 555).[43] Edge filters (Semrock) were used in front of the UV−vis fiber optic bundle to block the laser irradiation. The 532 nm excitation (20 mW at sample) was emitted from a solid state laser (Princeton Scientific, MSL 532-50), and the 325 nm excitation (5 mW at sample) was from a HeCd laser (Melles Griot). A UV-enhanced liquid-N_2-cooled CCD detector (Princeton Instruments) was employed for signal detection. The Raman reactor sits on an *XY* stage (Prior Scientific, OptiScan XY system) and translates in raster mode while collecting the spectrum. The fast translation has been shown to be able to eliminate/minimize any laser damage of adsorbed species on the samples. Cyclohexane was used as a standard for the calibration of the Raman shifts.

3. RESULTS AND DISCUSSION

3.1. Methanol Adsorption at Room Temperature.

Pulse chemisorption of methanol was conducted on the three ceria nanoshapes at room temperature. Figure 1 shows the IR spectra of one pulse of methanol adsorbed on ceria rods as a function of time. In the ν(CO) region, three bands grow conjointly at 1104, 1047, and 1032 cm^{-1} upon introduction of methanol, attributed to on-top methoxy (type I) and bridging methoxy (type II and II′) species, respectively.[2,23,25,32] The type II′ methoxy bridges Ce^{4+} cations having an oxygen vacancy in the neighborhood, but type II methoxy does not have an oxygen vacancy nearby.[23,25] At longer time (∼10 min) after the pulse, the 1104 cm^{-1} band dominates the ν(CO) region while a shoulder develops at around 1016 cm^{-1} due to three-coordinate methoxy (type III). Although the $\nu(CH_3)$ mode is less sensitive to the surface coordination than the ν(CO) mode, it is still helpful in determining the type of surface methoxy species.[23,32] As shown in Figure 1, two sharp bands at 2913 and 2802 cm^{-1} increase in intensity with adsorption time of methanol, assignable to asymmetric and symmetric CH_3 stretching modes of both on-top and bridging methoxy species, respectively. Three shoulders at 2942, 2886, and 2834 cm^{-1} are evident with the pair at 2942 and 2834 cm^{-1} as a result of physisorbed methanol and the band at 2886 cm^{-1} due to the overtone of CH_3 deformation mode ($2\delta(CH_3)$). The assignment of these bands is summarized in Table 1. In the ν(OH) region, negative-going OH bands are observed together with the development of a broad feature between 3000 and 3500 cm^{-1} due to hydrogen-bonded OH groups when surface methoxy groups are formed. The exact nature of surface OH groups on the ceria nanoshapes will be discussed in detail in a separate work.[44] The consumption of surface OH groups originates from their interaction (hydrogen bonding) with both the adsorbed methanol and the hydroxyls generated upon dissociative adsorption of methanol. It is also possible that some of the surface OH groups are replaced by methoxy species at room temperature[25] so that water-type species are produced, contributing to the broad feature above 3000 cm^{-1}.

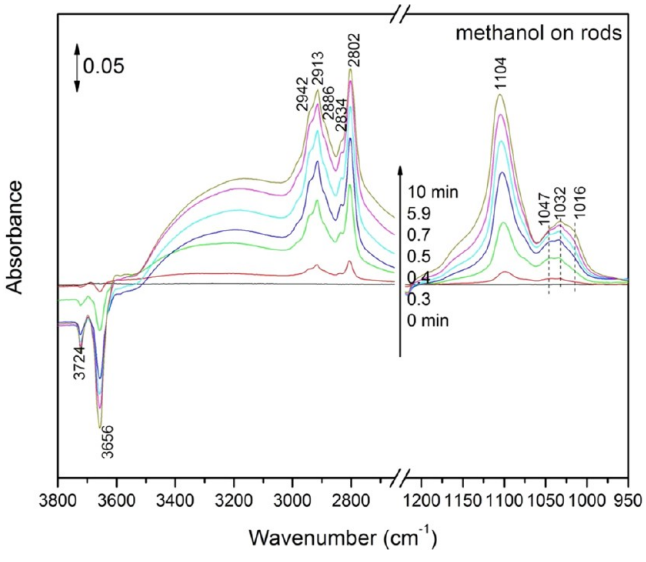

Figure 1. IR spectra following methanol adsorption on ceria rods at room temperature.

IR spectra from a methanol pulse on ceria cubes are exhibited in Figure 2. As indicated in the ν(CO) region, types I (1106 cm^{-1}), II (1077 cm^{-1}), and II′ (1037 cm^{-1}) methoxy species are formed upon methanol adsorption. Type III methoxy is also observable at the highest coverage (1019 cm^{-1}). It is notable that the percentage of bridging methoxy species (both types II and II′) relative to the on-top species increases on cubes in comparison with the case on rods. The IR peaks in the C−H stretching region can be grouped into three pairs on the basis of their growth trend: 2924 and 2805 cm^{-1} due to type II and III methoxy, 2916 and 2817 cm^{-1} due to type I methoxy, and 2945 and 2838 cm^{-1} due to physisorbed methoxy. The assignment is also aided by considering their relative IR band intensity and the relative amount of the three types of methoxy (from the C−O stretching region). The 2δ (CH_3) mode is also observed at 2886 cm^{-1}. Similar to that on ceria rods, methanol adsorption on cubes leads to the consumption of surface OH groups (negative going OH bands) and the production of hydrogen-bonded OH (broad feature between 3000 and 3500 cm^{-1}).

The IR spectra from methanol adsorption on ceria octahedra (Figure 3A) are somewhat surprising in the sense that the C−O stretching modes are barely observable but the C−H stretching peaks are pretty strong (or at least as strong as those observed on rods and cubes). The absence of strong ν(CO) features for ceria octahedra is not understood at this moment. A likely reason could be that the trace phosphate impurity strongly absorbs in the 1000−1100 cm^{-1} region, which warrants further investigation. A very weak peak at 1109 cm^{-1} may be resolved and is attributable to the presence of type I methoxy species. The two pairs of peaks in the C−H stretching region suggest the presence of physisorbed methanol (2943 and 2835 cm^{-1}) and possibly type I methoxy (2913 and 2806 cm^{-1}). Visible ($\lambda_{ex.}$ = 532 nm) Raman spectroscopy was employed to further investigate the methanol adsorption on the octahedra surface

dx.doi.org/10.1021/cs300467p | *ACS Catal.* 2012, 2, 2224−2234

Table 1. Assignment of IR Bands from Methanol Adsorption on Three Ceria Nanoshapes at Room Temperature

	Type I methoxy (percentage) 	Type II methoxy (percentage) 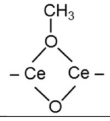	Type II' methoxy (percentage) 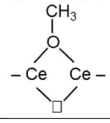	Type III methoxy (percentage) 	Physisorbed methanol
Rods {110}	1104 - ν(CO), 2802 - $\nu_s(CH_3)$, 2913 - $\nu_{as}(CH_3)$. (75%)	1047 - ν(CO), 2802 - $\nu_s(CH_3)$, 2913 - $\nu_{as}(CH_3)$ (3%)	1032 - ν(CO), 2802 - $\nu_s(CH_3)$, 2913 - $\nu_{as}(CH_3)$ (12%)	1016 - ν(CO), 2802 - $\nu_s(CH_3)$, 2913 - $\nu_{as}(CH_3)$ (10%)	1032 - ν(CO), 2834 - $\nu_s(CH_3)$, 2942 - $\nu_{as}(CH_3)$
Cubes {100}	1106, 2817, 2916. (43%)	1077, 2805, 2923. (5%)	1037, 2805, 2923. (40%)	1019, 2805, 2923. (12%)	1037, 2838, 2945.
Octahedra {111}	1109, 2806, 2913. (100%)	None	None	None	2835, 2943.

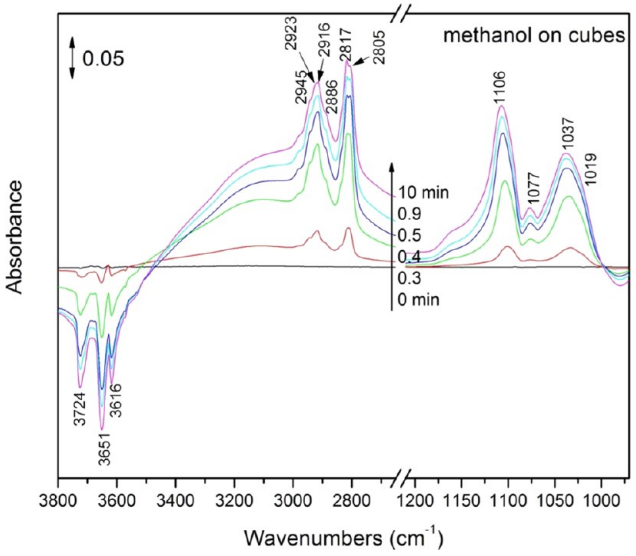

Figure 2. IR spectra following methanol adsorption on ceria cubes at room temperature.

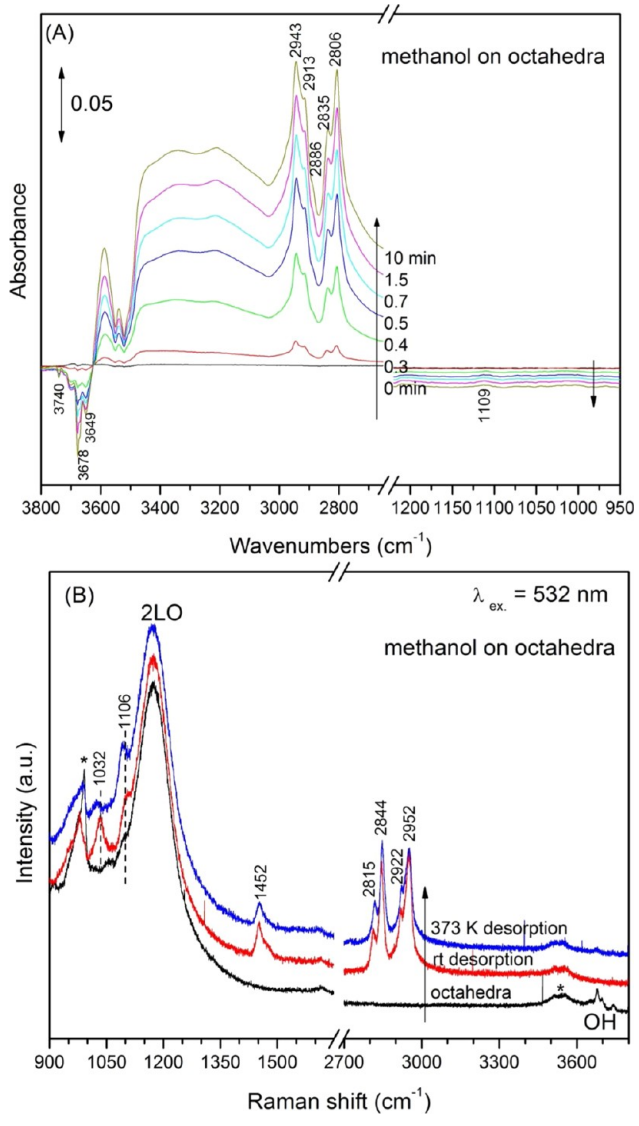

Figure 3. IR (A) and Raman (B) spectra following methanol adsorption on ceria octahedra at room temperature.

(Figure 3B). The background spectrum of ceria octahedra exhibits a sharp feature at ~991 cm^{-1} due to phosphate species, a broad feature centered at 1176 cm^{-1} due to the 2LO mode of ceria, and OH features at 3676 and 3740 cm^{-1}. When methanol was adsorbed on the octahedra, extra features were observed at 1032, 1106, 1452, 2815, 2844, 2922, and 2952 cm^{-1} while the ceria OH features disappeared. This is in accordance with the observation of negative-going OH groups in the IR spectra during methanol adsorption (Figure 3A), indicating the interaction between OH groups and adsorbed methanol species. The bands at 1106, 2815, and 2922 cm^{-1} can be assigned to type I methoxy species, and the bands at 1032, 2844, and 2952 cm^{-1} are due to physisorbed methanol. The reason for not assigning the 1032 cm^{-1} band to bridging methoxy is that it is less thermally stable than the band at 1106 cm^{-1} and decreased in intensity together with those of 2844 and 2952 cm^{-1} bands when the sample was heated to 373 K (see also below). It appears from both IR and Raman spectroscopy that only type I methoxy species are formed when methanol interacts with the octahedra. If any bridging

dx.doi.org/10.1021/cs300467p | ACS Catal. 2012, 2, 2224−2234

and three-coordinate methoxy are present, they are below the detection limit of Raman spectroscopy.

The adsorption of methanol on the three ceria nanoshapes was also monitored by UV (λ_{ex} = 325 nm) Raman spectroscopy. The spectra for the three nanoshapes before and after room temperature methanol adsorption are compared in Figure 4. No features due to adsorbed methanol species are

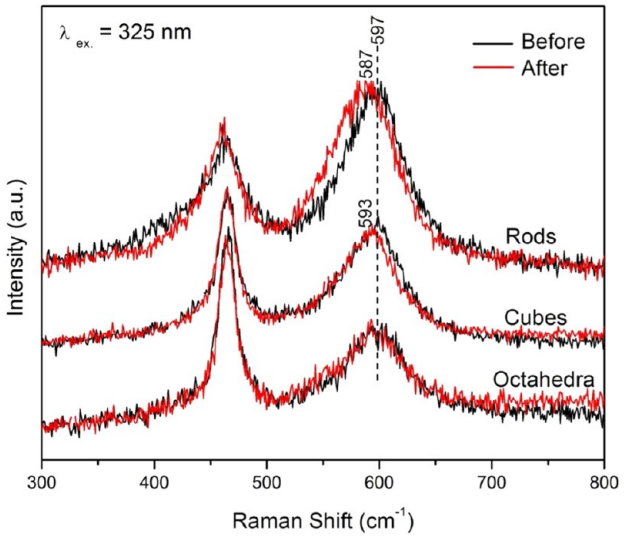

Figure 4. UV Raman spectra following methanol adsorption on ceria nanoshapes at room temperature.

observed using the 325 nm excitation because of the strong self-absorption of ceria in the UV region.[21,22] When the spectra are normalized to the F_{2g} mode (~464 cm^{-1}) of ceria, the D band at 597 cm^{-1} does not change in intensity after methanol adsorption, although it shifts to a lower frequency for rods and cubes . Similar shifts were observed in a previous study when the ceria nanoshapes were reduced by hydrogen at elevated temperatures, and the shifts were attributed to the generation of oxygen vacancies..[21,45] The shift upon methanol adsorption (10 cm^{-1}) for rods is less than that (32 cm^{-1}) generated by hydrogen reduction of rods at 673 K,[21] suggesting a lesser degree of reduction of ceria by methanol adsorption at room temperature. Judging from the shift of the D band, the extent of ceria reduction by methanol adsorption is the largest on the rods, followed by cubes and not detectable on octahedra. This trend is consistent with the oxygen vacancy formation energies of the nanoshapes' respective crystal surfaces: {110} < {100} < {111}.[46,47] A complicating factor is that Raman as a bulk technique is less sensitive to surface changes on the larger octahedra particles compared with rods and cubes.

Surface reduction by methanol adsorption was observed on a CeO_2{111} thin film using XPS[31−33] and on CeO_2{111} single crystal by STM.[29] Siokou et al.[32] explained the reduction at 300 K by a concerted radical-type mechanism for the dissociative adsorption of methanol on the ceria surface. Mullins et al.[31] observed the reduction of ceria by methanol, even at around 200 K, from both XPS (reduction of Ce^{4+} to Ce^{3+}) and TPD (desorption of water). Line defects were observed by STM when a CeO_2{111} surface was exposed to methanol at room temperature, which was attributed to the reduction of ceria via water formation.[29] Our result seems to support the explanation that the reduction is caused by the formation of water[29,31,33] through the reaction of surface OH groups whose hydrogen is produced from dissociated methanol. The broad feature in the range 3000−3500 cm^{-1} of the IR spectra (Figures 1−3) induced by methanol adsorption supports the formation of adsorbed water on the ceria surface.

Figure 5 shows a comparison of the IR spectra from methanol on the three ceria nanoshapes at room temperature.

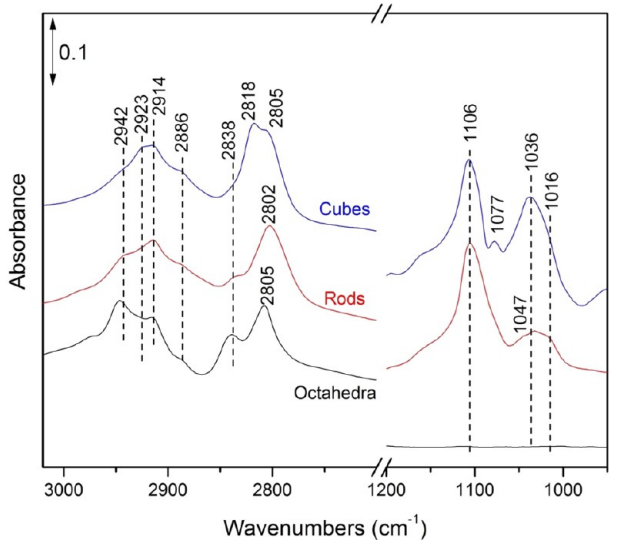

Figure 5. Comparison of IR spectra spectra following methanol adsorption on ceria nanoshapes at room temperature.

The spectra were obtained after room temperature purging in He. The type and distribution of methoxy species on the three nanoshapes are compared in Table 1. The relative amounts of the three types of methoxy species are estimated on the basis of their respective IR ν(CO) band area by assuming these methoxy species have similar IR absorption coefficients.[23] Two main distinctions in the type and distribution of the surface methoxy species can be made among the three ceria nanoshapes.

The Type of Methoxy Species. Type I methoxy is present on all three ceria surfaces, whereas bridging and three coordinate methoxy species are present only on the rods and cubes. Because the surface Ce cations are coordinatively unsaturated (namely, 7-coordination on {111} surface and 6-coordination on {110} (see Figure 6A and 6B)[28]), it is expected that on-top methoxy species can be formed upon dissociative adsorption of methanol on the rods and octahedra. For the {100} surface, it is generally assumed to be terminated with oxygen and is a polar surface (Figure 6C). Surface reconstruction has been suggested as a way to stabilize this polar surface by removing half of the oxygen from the surface (Figure 6D).[28,48,49] However, even on such a reconstructed {100} surface, it may be difficult to form an on-top methoxy on the Ce site because of the steric hindrance of the surface oxygen. Because our previous UV Raman study suggests the presence of defect sites on the ceria cubes,[21] it is possible that part of the{100} surface undergoes further reorganization, as suggested by Norenberg et al.,[49] so that some of the Ce cations are more exposed to allow the formation of on-top methoxy as well as multiply bonded ones. The bridging methoxy can be favorably formed on the reconstructed {100} surface.

The formation of type II and III methoxy species is not possible on the pristine {110} surface, and their formation has to be associated with the presence of defect sites on the rods'

dx.doi.org/10.1021/cs300467p | ACS Catal. 2012, 2, 2224−2234

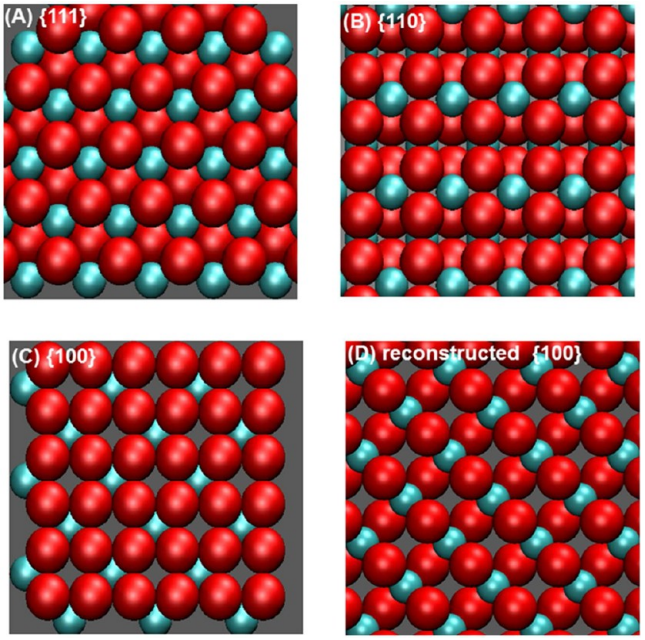

Figure 6. Structural models for (A) fully oxidized CeO_2{111}, (B) fully oxidized CeO_2{110}, (C) fully oxidized ideal {100}, and (D) fully oxidized reconstructed {100}. Red and light blue balls represent oxygen and cerium atoms, respectively.

surfaces.[21] It was shown by UV Raman and electron microscopy that more defect sites are available in ceria rods and cubes than in the octahedra.[21] For the {111} surface, the absence of bridging and three-coordinate methoxy species on the octahedral surface is consistent with the very limited number of defect sites on the octahedra surface as well as the steric interference of the first-layer oxygen anions. This contrasts with the observation of all three types of methoxy species on a CeO_2{111} thin film grown on Cu(111), which was explained by the presence of a certain amount of oxygen vacancies, as indicated by XPS.[32] It is possible that our ceria octahedra are fairly pristine with very few defects.

Previous UV Raman indicates the presence of a relatively small number of defect sites in the octahedra nanocrystals.[21] Because Raman is a bulk technique and the size of the octahedral particles is fairly large (83 nm), surface defect sites on the octahedra would be very limited. This is also supported by our recent study of the solid state reaction between vanadia and ceria nanoshapes, in which the lack of surface defect sites prevents the solid state reaction on octahedra while the reaction takes place facilely on the defective rods and cubes.[50] So it is reasonable that on-top methoxy is the predominant species observed on the ceria octahedra upon methanol adsorption.

The Distribution of Methoxy Species. There is a larger percentage of bridging methoxy (type II + II′) on the ceria cubes (45%) than on the rods (15%). This is reasonable because bridging sites are the most probable ones for methanol to adsorb on the reconstructed {100} surface[28,48] and, thus, are expected to dominate on the cubes' surface. The formation of bridging methoxy on a {110} surface is possible only when the rods' surface is defective, the extent of which is not expected to be as large as that resulting from the reconstruction of the {100} surface. It is also notable that among the multiply bonded methoxy species, bridging and three-coordinate methoxy are comparable in percentage on the rods. This is possibly related to the surface oxygen coordination number, which is 3 on the {110} surface,[28] It is sensible that three-coordinate methoxy would be present when some defect sites (O vacancies or steps) are available on the rods' surfaces.

3.2. Desorption and Reaction of Methanol at High Temperatures. *3.2.1. Methanol-TPD by Mass Spectrometer.* Methanol was adsorbed on the ceria samples at room temperature using the AMI microreactor system. The subsequent TPD profiles from ceria rods, cubes, and octahedra are shown in Figure 7A, B, and C, respectively. The major products on the three nanoshapes are H_2 and CO in the temperature range of 573−610 K. Other products include H_2O, methanol, and formaldehyde, and no appreciable CO_2 or $(CH_3)_2O$ is observed. The H_2 and CO originate from the complete dehydrogenation of methoxy via the reaction

$$\begin{aligned} &CH_3OH\ (g) + O_S \\ &\rightarrow CH_3O\ (a) + O_SH\ (a) \\ &\rightarrow CO\ (g) + 2H_2\ (g) + O_S \end{aligned} \quad (1)$$

where O_S represents a surface lattice oxygen of ceria and g and a denote gas phase and adsorbed species, respectively. The peak temperature for H_2 and CO is lower on ceria rods than on cubes and octahedra, an indication of stronger dehydrogenation capability of the rods. The CO peak generally appears at a slightly higher temperature than the H_2 peak, possibly suggesting a stepwise dehydrogenation process of methoxy on the three surfaces. This is more obvious for the cubes (Figure 7B), from which CO desorption peaks at 602 K, whereas H_2 peaks at 573 and 597 K. A possible explanation is that there are similar amounts of on-top and bridging methoxy on the cubes (Figure 2) and the different types of methoxy undergo dehydrogenation at different temperatures. The H/CO ratio was calculated by integrating the peak areas of H_2 + H_2O and CO and taking into consideration the mass spectrometer response factors for the three molecules. The ratio is ∼12.4, 9.2, and 5 for rods, cubes, and octahedra, respectively, all exceeding the stoichiometric ratio of 4 when methanol is completely dehydrogenated, as in reaction 1. These numbers indicate that as much as 2/3 of the carbon (for the rods) remains on the surface after desorption up to 703 K, likely in the form of formate and carbonate speciesm as evident in the IR study (Section 3.2.2).

Water is also observed to desorb from all three ceria surfaces with low temperature and high temperature desorption features. The low temperature water desorption starts around 340 K and peaks at 378, 403, and 414 K on rods, cubes, and octahedra, respectively. The low-temperature water is produced from the condensation reaction between surface OH groups that are generated from the dissociative adsorption of methanol on ceria.

$$2O_SH\ (a) \rightarrow H_2O_S\ (g) + O_S \quad (2)$$

The desorption of water signals the reduction of the ceria surface, and the desorption temperature on the three ceria nanoshapes is in general agreement with the trend in reducibility of the surfaces, that is, rods > cubes > octahedra.[20,47] The high temperature water desorption coincides with the desorption of CO from the three surfaces and originates from the oxidation (by ceria) of surface H cleaved from methoxy, thus also leading to surface reduction.

Desorption of a small amount of methanol and formaldehyde is observed at low temperature (<423 K) on all three ceria

dx.doi.org/10.1021/cs300467p | ACS Catal. 2012, 2, 2224−2234

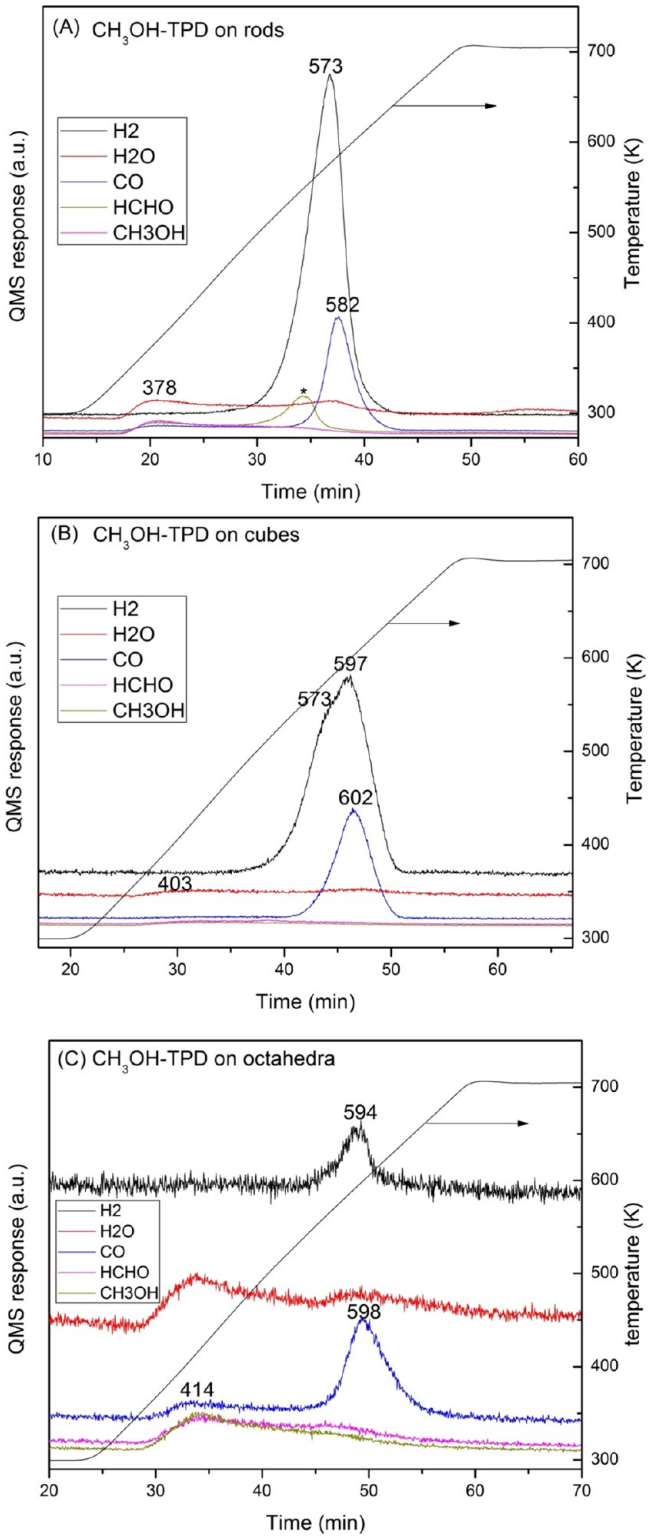

Figure 7. Methanol TPD profiles on ceria rods (A), cubes (B), and octahedra (C). The asterisk in part A denotes NO desorption from a nitrate impurity on the rods' surface.

surfaces, being less evident for the cubes. The similar intensity profiles of the two products indicate that methanol and formaldehyde are produced mainly from the disproportionation reaction of surface methoxy groups:

$$2CH_3O\ (a) \rightarrow CH_3OH\ (g) + HCHO\ (g) \qquad (3)$$

An anomalous peak at 550 K observed from the rods for mass 30 was determined to be NO originating from a nitrate impurity because no mass 29 is observed along with the mass 30.

3.2.2. In Situ Spectroscopy of Methanol Desorption. To understand the differences of the methanol-TPD profiles observed on the three ceria nanoshapes, the surface chemistry during methanol desorption was followed by in situ IR spectroscopy. The IR spectra obtained during methanol-TPD from ceria rods are shown in Figure 8. As shown before, the

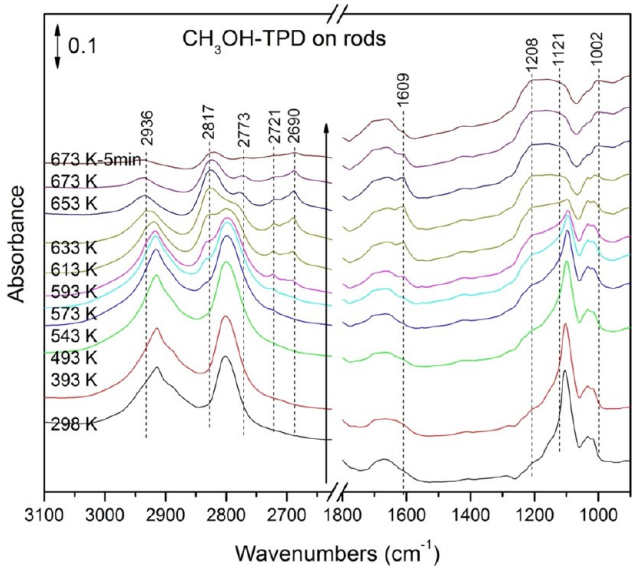

Figure 8. IR spectra during methanol TPD on ceria rods.

room temperature spectrum is characterized by C−H stretching modes at 2802 and 2913 cm^{-1}, and the C−O stretching modes, from three types of methoxy: namely, on-top (1104 cm^{-1}), bridging (1047 and 1032 cm^{-1}), and three-coordinate (1016 cm^{-1}). A broad feature is also observed between 1600 and 1700 cm^{-1}, attributable in part to the bending mode of adsorbed water. When heated in He to higher temperature, the IR band at 1104 cm^{-1} of the on-top methoxy gradually decreases in intensity relative to those of the bridging methoxy, indicating that the on-top methoxy species is less stable and more reactive on the ceria surface. This result is consistent with previous observations of methanol desorption or oxidation on ceria-based catalysts.[23,25,27] The on-top methoxy disappears by about 593 K, but the bridging methoxy is stable up to 653 K. The decrease of on-top methoxy parallels the creation of bidentate formate with characteristic bands at 2936 (δ(C−H) + ν_{as}(OCO)), 2817 (ν(C−H)), and 2721 (2δ(C−H)).[2,25,27] Its creation begins at 573 K and is described by reaction 4:

$$CH_3O\ (a) + O_S \rightarrow HCOO_S{-}\ (a) + H_2 \qquad (4)$$

It is unclear why the usually strong δ(C−H) and ν(OCO)) modes of formate are not observed in the range of 1600−1300 cm^{-1} on the rods' surface. At slightly higher temperature (593 K and above), new IR features appear at 2773 and 2690 cm^{-1} that could be assigned to formyl species.[51] Alternatively, these bands together with the new bands at 1609 and 1208 cm^{-1} could be ascribed to monodentate formate species,[2,27] but the latter assignment is not likely because the IR bands at 1208, 1609, 2690, and 2773 cm^{-1} are even more stable than those of the bidentate formate species and previous work showed that

dx.doi.org/10.1021/cs300467p | ACS Catal. 2012, 2, 2224−2234

monodentate formate is less stable than the bidentate formate on a ceria surface.[27]

Because the IR features due to formyl species appear at higher temperature than those of formate species (Figure 8), formyl species can also be considered as an intermediate in the decomposition of surface formate to give CO and H_2, which are the main desorption products in the methanol-TPD profiles:

$$HCOO_S-(a) \rightarrow O{=}CH-O_S-(a) \rightarrow CO\,(g) + (1/2)H_2\,(g) + O_S \quad (5)$$

It is noticeable that both the formyl and formate species are quite stable on the rods' surface and are still observable when heated up to 673 K. At 673 K, some extra IR features also persist at 1003, 1121, and 1208 cm^{-1} and between 1600 and 1700 cm^{-1}, which could be due to carbonate-like species produced by further oxidation of the formate species on the ceria surface.

IR spectra during methanol-TPD from ceria cubes are exhibited in Figure 9. Similar to the observation on the rods, the on-top methoxy is less stable than the bridging methoxy on the cubes, and formate species are created at the expense of the methoxy species starting at around 493 K. In contrast with the rods, there are two types of formate species formed on the cubes during the TPD process, characterized by different ν_{as}(OCO) modes at 1549 and 1585 cm^{-1}. The former mode is observed at lower temperature and attributed to bidentate formate species on the unreduced ceria surface (type I), and the latter one appears at higher temperature and is attributed to bidentate formate species adsorbed near an oxygen vacancy (type II).[2,25] The IR band at 1585 cm^{-1} becomes the major ν_{as}(OCO) mode at a temperature higher than 533 K, indicating more reduction of cubes at higher temperature. Other IR features are observed at 1328 (ν_s(OCO)), 1367 (δ(C−H)), 2720 (2δ(C−H)), 2833 (ν(C−H)), and 2936 cm^{-1} (δ(C−H) + ν_{as}(OCO)). They grow in intensity together with the ν_{as}(OCO) modes and are thus also associated with the two formate species. No IR features due to formyl species are present during the desorption process. Some formate species are still present on the cubes, even after 673 K desorption, and some of the remaining features (1585, 1431, and 1328 cm^{-1}) could be due to carbonate species, as was also seen on the rods.

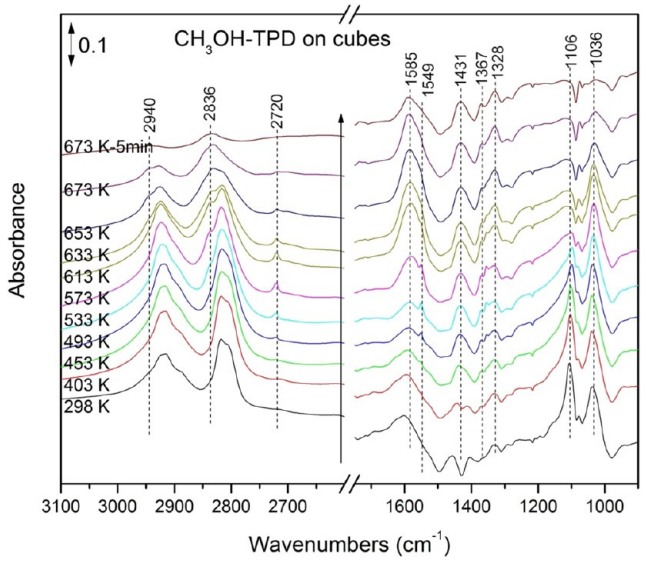

Figure 9. IR spectra during methanol TPD on ceria cubes.

Figure 10A presents the IR spectra collected during methanol-TPD from ceria octahedra. In this case, the CH_3 stretching modes are used to follow the stability of the methoxy species due to inability to detect the ν(CO) mode on octahedra. Since the $\nu_s(CH_3)$ mode of physisorbed methanol and the $\nu_{as}(CH_3)$ mode of methoxy species happen to coincide with the vibrational modes of the produced formate species, the physisorbed methanol species is tracked with its $\nu_{as}(CH_3)$ mode at 2950 cm^{-1} and the on-top methoxy is tracked by its $\nu_s(CH_3)$ mode at 2810 cm^{-1}. Apparently, the physisorbed methanol desorbs below 473 K, and the on-top methoxy species is stable up to 623 K. Formate species are produced as the surface methoxy species is consumed. Type I formate is exclusively formed starting at 453 K because a single ν_{as}(OCO) mode is observed at 1545 cm^{-1}. Type II formate, characterized by the ν_{as}(OCO) mode at 1583 cm^{-1}, appears at higher temperature and continues to increase in intensity. In contrast to the case for cubes for which type II formate species dominates over type I, the two formate species are comparable

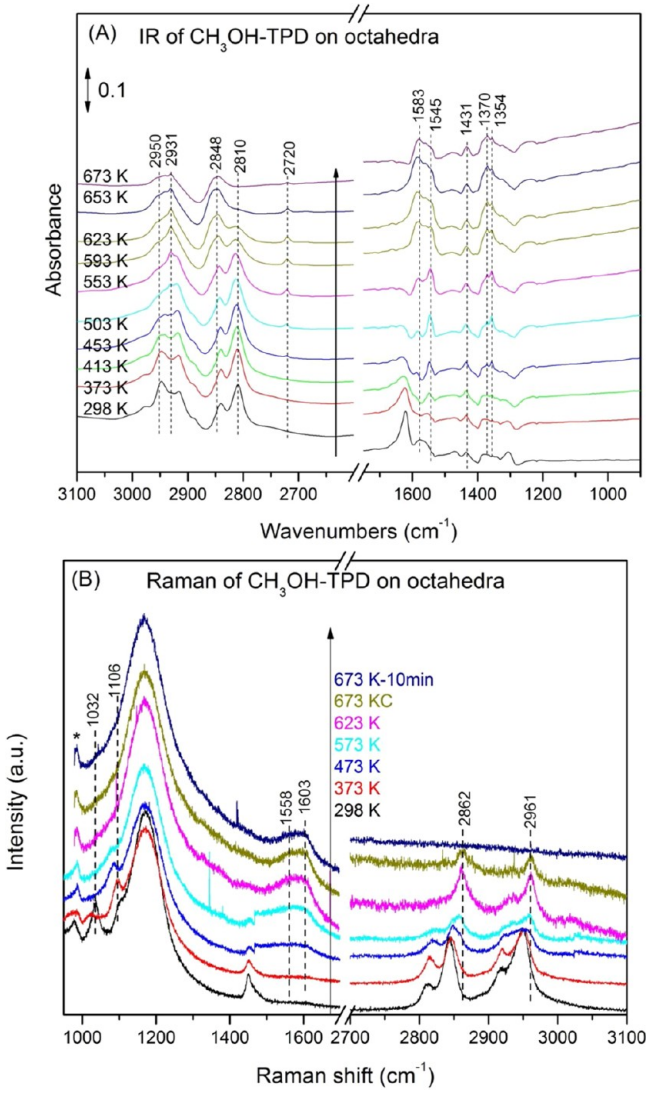

Figure 10. IR (A) and Raman (B) spectra during methanol-TPD on ceria octahedra.

dx.doi.org/10.1021/cs300467p | ACS Catal. 2012, 2, 2224−2234

in amount on octahedra when the desorption temperature is up to 673 K, indicating less reduction of the octahedra surface than the cubes. Again, all IR features at high desorption temperature can be ascribed to formate species and carbonate-like species with no sign of formyl species.

Since Raman spectroscopy is able to detect the ν(CO) mode on octahedra surface, the methanol-TPD process was also followed by Raman spectroscopy, as shown in Figure 10B. The temperatures marked in the Raman spectra are not expected to match those in the IR spectra for two reasons: (a) different in situ reactors were used in the IR and Raman studies and (b) the Raman TPD was done in a ramp-and-hold mode to allow the collection (taking ∼5 min) of Raman spectra at a specific temperature, whereas the IR TPD was done in a continuous ramping mode. As illustrated in Figure 10B, two ν(CO) modes are observed at 1032 and 1106 cm^{-1} on octahedra after methanol adsorption at room temperature. Upon heating to 373 K, the band at 1032 cm^{-1} decreases in intensity relative to the 1106 cm^{-1} band. Further heating to 473 K eliminates the 1032 cm^{-1} band while the band at 1106 cm^{-1} (slightly shifted to lower frequency) still persists. The relative thermal stability of the two bands indicates that the band at 1032 cm^{-1} is not due to type II methoxy but, rather, is due to physisorbed methanol. The type I methoxy is stable up to 573 K; its Raman bands at 1106, 2804, and 2918 cm^{-1} are still observable at this temperature. Meanwhile, Raman features due to two types of formate species grow as the methoxy species are consumed. Two ν_{as}(OCO) modes are observed at 1558 and 1603 cm^{-1} for types I and II formate species, respectively. The type II band at 1603 cm^{-1} (related to oxygen vacancies) is slightly more intense than the one at 1558 cm^{-1}, similar to the IR observation (Figure 10A) and signaling the reduction of the surface. Other features at 2862 and 2961 cm^{-1} are also attributed to the formate species. The ν_{as}(OCO) modes persist at 673 K, implying that the two formate species are thermally stable, in agreement with the IR result.

The in situ spectroscopy results (Figures 8−10) on the ceria rods, cubes, and octahedra can lend some insights into the desorption product profiles (Figure 7):

(a) The IR results suggest that formate is an intermediate in the generation of H_2 and CO, which are the major desorption products. On ceria rods, another surface species, formyl was found as an intermediate from formate decomposition to H_2 and CO. It seems that the {110} surface of ceria is necessary in stabilizing the formyl species, the underlying mechanism of which is not yet understood.

(b) The high H/CO ratio (>4) observed on the three surfaces is due to the retention of carbon-related species on the surface, even at 673 K, as shown by IR spectra. These include formate and possibly carbonates that are produced by reaction of CO/CO_2 (from formate decomposition) with ceria surface oxygen. The higher ratio of H/CO desorption products on rods could be related to the higher thermal stability of formate, formyl, and carbonate on rods. For formate and formyl, their higher stability on rods than on cubes and octahedra can be judged from the observation of IR features in the C−H stretching region at 673 K (the OCO stretching region is mixed with carbonates) (Figures 8−10). The stability of carbonate species resulting from CO adsorption was shown to follow the trend, rods > cubes > octahedra.[20] This trend agrees with the observed trend in ratio of the desorbed H/CO on the three ceria nanoshapes; namely, rods (12.4) > cubes (9.2) > octahedra (5).

(c) The low temperature shoulder at 573 K of the H_2 desorption peak (Figure 7B) on cubes may be related to the presence of type I formate, which is present only in the intermediate temperature range, whereas the type II formate, contributing to the main H_2 peak, dominates and persists to higher temperature on cubes. The absence of a corresponding shoulder on the CO desorption peak on cubes indicates that the CO species from the decomposition of type I formate may be strongly adsorbed or converted into carbonate-like species on the cubes' surface. Although two types of formate species are also present on the octahedral surface, IR spectra (Figure 10A) show that the two appear to be similarly stable on the surface, and thus, only one main H_2 desorption peak is observed. Therefore, the adsorption strength and reactivity of the formate species are dependent on the surface structure of the ceria nanocrystals. An alternative explanation for the two desorption temperatures of H_2 on cubes could be that the {100} surface stabilizes two intermediate steps in the sequential dehydrogenation process of methoxy, leading to separation of H_2 desorption on cubes.

(d) The gradual decrease of on-top methoxy species starting at 373 K supports the disproportionation reaction of methoxy to produce methanol and formaldehyde, as observed in the methanol-TPD profiles in the temperature range of 373−423 K on the three ceria nanoshapes. It is reasonable that the type I methoxy species participates in this reaction at such low temperature because it is the least stable among the three types of methoxy species on ceria surfaces.

Putting the current study into perspective, it is useful to compare the methanol-TPD results on the ceria nanoshapes with those in the current literature. The most available literature studies of methanol adsorption on ceria with well-defined surface structure are on a CeO_2{111} single crystal[29,30] or thin films.[30−33] On a pristine CeO_2{111} single crystal or thin film, the primary desorption productions from methanol adsorption are formaldehyde, methanol, and water,[30,31] but they shift to H_2 and CO when the ceria surface is defective[32] or reduced.[30−32] On the ceria octahedra surface ({111} terminated), methanol desorption gives mainly H_2 and CO, in good agreement with the observation made on a defective CeO_2{111} single crystal or thin film. This is not surprising because our previous UV Raman study showed the presence of defect sites in ceria octahedra. Although the majority of defects may be located inside the bulk of octahedra, they can become mobile at high temperatures[20] and, thus, contribute to the dehydrogenation of methoxy species into H_2 and CO, as observed in the methanol-TPD profiles.

There was only one study of methanol adsorption on CeO_2{100} thin film supported on YSZ{100}.[30] This ceria thin film was not fully oxidized and so contained Ce^{3+} cations. Methanol desorption on this CeO_2{100} surface resulted in production of H_2, CO, H_2O, CH_3OH, and HCHO. Our result on the ceria cubes ({100} terminated) is in general agreement with this. Furthermore, because of the presence of a rather large number of defect sites[21] and surface reconstruction,[48] it is reasonable that H_2 and CO are the primary products from the

cubes' surface. Although there is no available study of CeO_2{110} single crystals or thin films, the major TPD products on ceria rods (containing {110} facet) are H_2 and CO, similar to those on cubes and octahedra and confirming the defective nature of the rods' surface as revealed by Raman and electron microscopy.[20,21]

Another contributing factor to the observation of H_2 and CO as major desorption products on the ceria nanoshapes is readsorption. Multiple desorption, readsorption, and secondary reaction can occur on the powdered ceria samples loaded in a microreactor environment during methanol-TPD. These secondary reactions can lead to the decomposition of any dehydrogenated intermediate product, such as formaldehyde. In a UHV environment, rapid pumping and the use of a flat film or single crystal surfaces ensure that the product desorption is a one-time event.

4. CONCLUSIONS

In situ IR and Raman spectroscopy have been employed to investigate the surface chemistry during methanol adsorption and reaction on three ceria nanoshapes, rods, cubes, and octahedra. Methanol adsorption at room temperature leads to different types of methoxy species, that is, on-top, bridging, and three-coordinate methoxy on the three surfaces. The distribution of these methoxy species is dependent on the shape (surface structure) of the ceria nanocrystals as well as the number of defect sites on them. Slight reduction of the rods' and cubes' surfaces is observed at room temperature upon methanol adsorption by the UV Raman study. Upon desorption at elevated temperature, H_2 and CO are the main products on the three ceria nanoshapes, and their desorption temperature and relative ratio are dependent on the shape of the ceria nanocrystals. The in situ spectroscopy study shows that H_2 and CO are formed by dehydrogenation of the methoxy species via formate species as one of the reaction intermediates. The presence of two types of formate species implies the reduction of the ceria surface upon methanol reaction at high temperatures. Some formate and possibly carbonate species are retained on the ceria nanoshapes after high-temperature desorption, explaining the higher than stoichiometric H/CO ratio observed in the methanol-TPD products. The results presented here suggest that although the three ceria nanoshapes are well-structured on the surface, they also contain defects on the surface and in the bulk that can have a profound effect on the surface chemistry during ceria catalysis.

AUTHOR INFORMATION

Corresponding Author

*(Z.W.) Phone: 1-865-576-1080. E-mail: wuz1@ornl.gov. (S.H.O.) E-mail: overburysh@ornl.gov.

Author Contributions

The manuscript was written through contributions of all authors. All authors have given approval to the final version of the manuscript.

Notes

The authors declare no competing financial interest.

ACKNOWLEDGMENTS

This Research is sponsored by the Division of Chemical Sciences, Geosciences, and Biosciences, Office of Basic Energy Sciences, U.S. Department of Energy. Part of the work, including the Raman study, was conducted at the Center for Nanophase Materials Sciences, which is sponsored at Oak Ridge National Laboratory by the Scientific User Facility Division, Office of Basic Energy Science, U.S. Department of Energy. The research was supported in part by the appointment for M.J.L. to the ORNL Postdoctoral Research Associates Program, administered jointly by ORNL and the Oak Ridge Associated Universities.

REFERENCES

(1) Trovarelli, A. *Catal. Rev.—Sci. Eng.* **1996**, *38*, 439−520.
(2) Binet, C.; Daturi, M.; Lavalley, J. C. *Catal. Today* **1999**, *50*, 207−225.
(3) Vivier, L.; Duprez, D. *ChemSusChem* **2010**, *3*, 654−678.
(4) Beckers, J.; Rothenberg, G. *Green Chem.* **2010**, *12*, 939−948.
(5) Ratnasamy, C.; Wagner, J. P. *Catal. Rev.—Sci. Eng.* **2009**, *51*, 325−440.
(6) Duprez, D.; Descorme, C.; Birchem, T.; Rohart, E. *Top. Catal.* **2001**, *16*, 49−56.
(7) Rodriguez, J. A.; Ma, S.; Liu, P.; Hrbek, J.; Evans, J.; Perez, M. *Science* **2007**, *318*, 1757−1760.
(8) Guzman, J.; Carrettin, S.; Corma, A. *J. Am. Chem. Soc.* **2005**, *127*, 3286−3287.
(9) Si, R.; Flytzani-Stephanopoulos, M. *Angew. Chem., Int. Ed.* **2008**, *47*, 2884−2887.
(10) Esch, F.; Fabris, S.; Zhou, L.; Montini, T.; Africh, C.; Fornasiero, P.; Comelli, G.; Rosei, R. *Science* **2005**, *309*, 752−755.
(11) Zhou, K. B.; Wang, X.; Sun, X. M.; Peng, Q.; Li, Y. D. *J. Catal.* **2005**, *229*, 206−212.
(12) Mai, H. X.; Sun, L. D.; Zhang, Y. W.; Si, R.; Feng, W.; Zhang, H. P.; Liu, H. C.; Yan, C. H. *J. Phys. Chem. B* **2005**, *109*, 24380−24385.
(13) Yan, L.; Yu, R. B.; Chen, J.; Xing, X. R. *Cryst. Growth Des.* **2008**, *8*, 1474−1477.
(14) Tana; Zhang, M. L.; Li, J.; Li, H. J.; Li, Y.; Shen, W. J. *Catal. Today* **2009**, *148*, 179−183.
(15) Liu, X. W.; Zhou, K. B.; Wang, L.; Wang, B. Y.; Li, Y. D. *J. Am. Chem. Soc.* **2009**, *131*, 3140−3041.
(16) Guan, Y. J.; Hensen, E. J. M.; Liu, Y.; Zhang, H. D.; Feng, Z. C.; Li, C. *Catal. Lett.* **2010**, *137*, 28−34.
(17) Lin, K. S.; Chowdhury, S. *Int. J. Mol. Sci.* **2010**, *11*, 3226−3251.
(18) Han, W. Q.; Wen, W.; Hanson, J. C.; Teng, X. W.; Marinkovic, N.; Rodriguez, J. A. *J. Phys. Chem. C* **2009**, *113*, 21949−21955.
(19) Zhang, J.; Kumagai, H.; Yamamura, K.; Ohara, S.; Takami, S.; Morikawa, A.; Shinjoh, H.; Kaneko, K.; Adschiri, T.; Suda, A. *Nano Lett.* **2011**, *11*, 361−364.
(20) Wu, Z. L.; Li, M. J.; Overbury, S. H. *J. Catal.* **2012**, *285*, 61−73.
(21) Wu, Z. L.; Li, M. J.; Howe, J.; Meyer, H. M.; Overbury, S. H. *Langmuir* **2010**, *26*, 16595−16606.
(22) Taniguchi, T.; Watanabe, T.; Sugiyama, N.; Subramani, A. K.; Wagata, H.; Matsushita, N.; Yoshimura, M. *J. Phys. Chem. C* **2009**, *113*, 19789−19793.
(23) Badri, A.; Binet, C.; Lavalley, J. C. *J. Chem. Soc. Faraday Trans.* **1997**, *93*, 1159−1168.
(24) Badri, A.; Binet, C.; Lavalley, J. C. *J. Chem. Soc. Faraday Trans.* **1997**, *93*, 2121−2124.
(25) Rousseau, S.; Marie, O.; Bazin, P.; Daturi, M.; Verdier, S.; Harle, V. *J. Am. Chem. Soc.* **2010**, *132*, 10832−10841.
(26) Binet, C.; Daturi, M. *Catal. Today* **2001**, *70*, 155−167.
(27) Li, C.; Domen, K.; Maruya, K.; Onishi, T. *J. Catal.* **1990**, *125*, 445−455.
(28) Ganduglia-Pirovano, M. V.; Hofmann, A.; Sauer, J. *Surf. Sci. Rep.* **2007**, *62*, 219−270.
(29) Namai, Y.; Fukui, K.; Iwasawa, Y. *Nanotechnology* **2004**, *15*, S49−S54.
(30) Ferrizz, R. M.; Wong, G. S.; Egami, T.; Vohs, J. M. *Langmuir* **2001**, *17*, 2464−2470.
(31) Mullins, D. R.; Robbins, M. D.; Zhou, J. *Surf. Sci.* **2006**, *600*, 1547−1558.
(32) Siokou, A.; Nix, R. M. *J. Phys. Chem. B* **1999**, *103*, 6984−6997.

(33) Matolin, V.; Libra, J.; Skoda, M.; Tsud, N.; Prince, K. C.; Skala, T. *Surf. Sci.* **2009**, *603*, 1087−1092.
(34) Mei, D.; Deskins, N. A.; Dupuis, M.; Ge, Q. F. *J. Phys. Chem. C* **2008**, *112*, 4257−4266.
(35) Mei, D.; Deskins, N. A.; Dupuis, M.; Ge, Q. *J. Phys. Chem. C* **2007**, *111*, 10514−10522.
(36) Beste, A.; Mullins, D. R.; Overbury, S. H.; Harrison, R. J. *Surf. Sci.* **2008**, *602*, 162−175.
(37) Chowdhury, S.; Lin, K. S. *Mater. Chem. Phys.* **2012**, *133*, 163−169.
(38) Granados, M. L.; Galisteo, F. C.; Lambrou, P. S.; Manscal, R.; Sanz, J.; Sobrados, I.; Fierro, J. L. G.; Efstathiou, A. M. *J. Catal.* **2006**, *239*, 410−421.
(39) Wu, Z. L.; Schwartz, V.; Li, M. J.; Rondinone, A. J.; Overbury, S. H. *J. Phys. Chem. Lett.* **2012**, *3*, 1517−1522.
(40) Wu, Z. L.; Zhou, S. H.; Zhu, H. G.; Dai, S.; Overbury, S. H. *J. Phys. Chem. C* **2009**, *113*, 3726−3734.
(41) Wu, Z. L.; Zhou, S. H.; Zhu, H. G.; Dai, S.; Overbury, S. H. *Chem. Commun.* **2008**, 3308−3310.
(42) Li, M. J.; Wu, Z. L.; Ma, Z.; Schwartz, V.; Mullins, D. R.; Dai, S.; Overbury, S. H. *J. Catal.* **2009**, *266*, 98−105.
(43) Wu, Z. L.; Dai, S.; Overbury, S. H. *J. Phys. Chem. C* **2010**, *114*, 412−422.
(44) Wu, Z. L.; Li, M. J.; Overbury, S. H. **2012**, In preparation.
(45) Lee, Y.; He, G. H.; Akey, A. J.; Si, R.; Flytzani-Stephanopoulos, M.; Herman, I. P. *J. Am. Chem. Soc.* **2011**, *133*, 12952−12955.
(46) Nolan, M.; Fearon, J. E.; Watson, G. W. *Solid State Ionics* **2006**, *177*, 3069−3074.
(47) Nolan, M.; Parker, S. C.; Watson, G. W. *Surf. Sci.* **2005**, *595*, 223−232.
(48) Conesa, J. C. *Surf. Sci.* **1995**, *339*, 337−352.
(49) Norenberg, H.; Harding, J. H. *Surf. Sci.* **2001**, *477*, 17−24.
(50) Wu, Z. L.; Li, M. J.; Overbury, S. H. *ChemCatChem* **2012**, DOI: 10.1002/cctc.201200243.
(51) Li, C.; Sakata, Y.; Arai, T.; Domen, K.; Maruya, K. I.; Onishi, T. *J. Chem. Soc. Faraday Trans. I* **1989**, *85*, 1451−1461.